436 | https://doi.org/10.3311/PPci.43221
Creative Commons Attribution

Periodica Polytechnica Civil Engineering, 70(2), pp. 436–455, 2026

Multi-objective Static-dynamic Scheduling for Dual-tunnel Construction under Spatiotemporal Constraints

Yu Li Tian[1], Lei Wang[1*], Jin Kun Huang[2], An Bin Wang[1], An Chun Cheng[2]

[1] Department of Railway Engineering, School of Urban Railway Transportation, Shanghai University of Engineering Science, No. 333 Longteng Road, Songjiang District, 201620 Shanghai, China
[2] China MCC17 Group Co., LTD., No. 88 Yushan East Road, 243000 Ma'anshan, Anhui, China
[*] Corresponding author, e-mail: wangleiwangjiang@163.com

Received: 30 December 2025, Accepted: 21 March 2026, Published online: 23 April 2026

Abstract

This study develops a high-fidelity multi-objective static and dynamic scheduling model for dual-tunnel construction. To overcome topological deadlocks in tightly restricted spaces, complemented by a fine-grained time-slice mapping mechanism to eliminate resource fragmentation. At the static level, the optimization aims to minimize both the total make-span and the Weighted Resource Fluctuation Standard Deviation. A Memetic Algorithm-based Hybrid Genetic Algorithm (HGA) is proposed to solve the NP-hard problem. The algorithmic engine is fundamentally upgraded by incorporating an unbiased topological sequence initialization to expand the early exploration space, a dynamic continuity penalty function to ensure intra-cycle operational fluidity, and an elite local search strategy to overcome genetic hardening. Furthermore, the ε-constraint method is utilized to extract the exact Pareto front. An application to a 100-meter dual-tunnel engineering case demonstrates that the proposed HGA possess significant global optimization capabilities, while the rolling-horizon dynamic scheduling exhibits superior computational efficiency. The static optimization reduced the construction duration by 13.3% compared to the actual schedule, while the dynamic optimization achieved a 11.5% reduction under ideal conditions. Furthermore, disturbance simulation experiments confirm that this dynamic scheduling mechanism maintains a linear and stable increase in predicted duration across various disturbance scenarios, demonstrating excellent stability and robustness.

Keywords

dual-tunnel repetitive project scheduling, hybrid genetic algorithm, rolling horizon optimization, multi-objective optimization, dynamic scheduling

1 Introduction

Over the past three decades, the construction of expressways has driven China's rapid development. As of the end of 2024, the total mileage of highways in China reached 5.49 million kilometers, including 28724 highway tunnels with a total length of 32.5966 million linear meters [1]. Among these, dual-tunnel configurations have become the mainstream model for constructing long, large tunnels due to their ability to effectively increase traffic capacity, alleviate traffic pressure on single tunnels, and improve operational safety. Therefore, dynamically adjusting tunnel construction schedules and balancing overall resource demands while ensuring construction safety is of significant research importance.

The scheduling of such linear infrastructure is classically referred to as the Repetitive Project Scheduling Problem (RPSP). Early studies predominantly relied on the Linear Scheduling Method (LSM) to describe operational relationships within a two-dimensional spatio-temporal coordinate system [2]. While LSM provides an intuitive representation, it lacks the ability to optimize complex resource constraints effectively. To address this, subsequent research introduced mathematical programming and metaheuristic algorithms [3–5]. As engineering complexity increases, research focus has shifted from single-objective to multi-objective optimization, aiming to trade off conflicting goals such as time, cost, and resources [6–15]. For instance, Dede et al. [9] have integrated the NDS-II framework with best-mean-random (BMR) and best-worst-random (BWR) strategies to minimize total project time and cost while reducing overall safety risks. Similarly, strength Pareto-based Rao algorithms (SP2-Rao-1 and -2) have been proposed as an

Cite this article as: Tian, Y. L., Wang, L., Huang, J. K., Wang, A. B., Cheng, A. C. "Multi-objective Static-dynamic Scheduling for Dual-tunnel Construction under Spatiotemporal Constraints", Periodica Polytechnica Civil Engineering, 70(2), pp. 436–455, 2026. https://doi.org/10.3311/PPci.43221

effective approach to solving multi-objective time–cost–quality problems in construction projects [10]. Algorithms such as NSGA-II and MOPSO have been widely applied to tunnel alignment optimization [11], renovation planning for historic blocks [12], and the comprehensive trade-off among resource-duration-cost [13–17]. Su and Aviles [6] proposed a bi-objective optimization model to minimize construction duration and resource fluctuations, developing an Improved Whale Optimization Algorithm (IWOA) to solve it. Guo and Zhang [11] used the Non-dominated Sorting Genetic Algorithm-II (NSGA-II) to optimize tunnel alignment, focusing on investment, spacing, and comfort. Ren and Zhang [12] proposed a multi-objective optimization method for the renovation of historic and cultural blocks, improving the NSGA-II algorithm with chaotic mapping and differential mutation strategies.

Furthermore, as single algorithms struggle to adapt to all engineering problems, novel swarm intelligence algorithms—such as hybrid algorithms and multi-strategy improved algorithms—continue to emerge across diverse engineering domains [18–28]. In structural engineering, a multi-objective colliding bodies optimization (MOCBO) algorithm was proposed to solve the multi-objective optimization problems of truss structures [16]. Additionally, performance-based seismic optimization design methods for steel frame structures have been presented, utilizing programming software to realize automated calculations [17]. To further enhance algorithmic efficiency in these performance-based problems, Kaveh et al. [18] have employed NSGA-II using differential evolution operators. Hu et al. [21] proposed a hybrid optimization method combining an improved Genetic Algorithm (GA) with time-varying mutation rates and Particle Swarm Optimization (PSO). Similarly, Zou and Zhou [22] developed a scheduling model for beam erection engineering and proposed a hybrid Tabu-Variable Neighborhood Genetic Algorithm incorporating multiple strategies. Hybrid strategies have also been applied to construction site layout planning, such as combining the Dragonfly Algorithm (DA) with PSO [21], and integrating the Gravitational Search Algorithm (GSA) with Thermal Exchange Optimization (TEO) [22]. Additionally, a Chaotic Improved Whale Optimization Algorithm with Backpropagation (CIWOA-BP) was used to optimize the welding sequence of complex structural components [24], and a Sampling Heuristic Initialization-based Particle Swarm (SHI-PSO) algorithm was developed to balance speed and quality in path planning [25]. Improved multi-strategy Snake Optimization algorithms [26] and an adaptive version of the Snake Optimization (SO) algorithm employing chaotic reverse learning and opposition-based learning [23] have achieved success in diverse fields, ranging from unmanned aerial vehicle (UAV) path planning to wireless sensor network node deployment and any other engineering optimization tasks.

Despite significant progress in static optimization, traditional methods have limitations when applied to the construction of dual tunnels. First, existing studies often treat tunnels as independent units, inadequately modeling the unique dual-tube interaction constraints. Specifically, insufficient consideration of the particularities of dual-tunnel parallel construction makes it challenging to characterize limitations, such as the coupling of operations between the left and right tubes and the competition for shared resources (e.g., equipment and specialized crews). Second, tunnel construction is inherently uncertain and frequently subject to dynamic disturbances such as abrupt changes in geological conditions, equipment failures, or policy-driven schedule compression. In such a volatile environment, static schedules, however optimal theoretically, often become infeasible in practice, leading to resource waste and safety risks.

To address construction uncertainty, dynamic scheduling methods based on Rolling Horizon Optimization (RHO), Reinforcement Learning (RL), and improved heuristic algorithms have gained attention in other fields [27–32]. For example, RHO has been used to manage stochastic loads in energy systems [27], and dynamic models have been applied to earthwork equipment configuration [31]. Cheng et al. [29] adopted Rolling Horizon Optimization to address the stochastic nature of loads and renewable energy sources. Wei et al. [31] established a time-cost multi-objective optimization model for critical equipment configuration based on the NSGA-II algorithm and entropy weight TOPSIS decision-making; they developed a comprehensive equipment configuration method for the entire drill-and-blast tunnel construction process, accounting for tunnel cross-section type, surrounding rock conditions, excavation length, and construction schedule requirements. Khallaf et al. [33] introduced a Mixed Integer Linear Programming (MILP) model to determine the optimal configuration of heavy equipment in earthwork operations, incorporating dynamic characteristics to enable daily progress updates based on available resources. Wei et al. [34] developed a dynamic optimization model for tunnel construction scheduling, which

analyzes logical relationships, work continuity, spatiotemporal constraints, and resource variations.

However, research specifically targeting the dynamic scheduling of dual-tunnel parallel construction remains limited. There is an urgent need for an integrated dynamic scheduling optimization framework capable of simultaneously generating a high-quality global baseline schedule and robustly responding to real-time disturbances while satisfying the complex spatiotemporal constraints of dual-tunnel operations.

To address the aforementioned gaps and specifically overcome the critical failure of generic metaheuristics in highly constrained underground environments, this study transcends traditional integrative applications by proposing a customized, dual-layer static-dynamic scheduling framework. The fundamental novelties and primary contributions of this research are highlighted as follows:

1. *Mathematical formulation of dual-tube spatiotemporal coupling constraints*: Moving beyond generic Resource-Constrained Project Scheduling Problem (RCPSP) paradigms, this study explicitly formulates the complex physical realities of dual-tunnel parallel construction. By mathematically modeling the strict spatial staggered distances, e.g., the 30 m safety lag between left and right tubes, and the continuous spatial boundary locks among excavation, invert, and secondary lining, the proposed model perfectly captures the unique topological dependencies that standard independent-tunnel scheduling models inherently fail to represent.
2. *Architecture of a domain-specific Hybrid Genetic Algorithm (HGA)*: Standard continuous swarm intelligence algorithms and generic discrete metaheuristics suffer from catastrophic topological feasibility collapse when applied to rigid dual-tunnel constraints. To conquer this, we structurally customized the HGA with a Cycle-Aware Topological Initialization and a Workflow-Similarity-Based Smart Mutation. These domain-specific operators inherently immunize the evolutionary process against cycle-breaking penalties, guaranteeing near 100% sequence feasibility and demonstrating overwhelming algorithmic superiority over state-of-the-art methods (e.g., MOWOA, PSO) in unlocking the absolute physical minimum makespan.
3. *Engineering-driven ε-constraint multi-objective strategy*: We reveal and theoretically resolve the idle penalty trap inherent in simultaneous bi-objective optimization, e.g., NSGA-II, where algorithms artificially delay critical tasks merely to achieve mathematical resource variance smoothing. By employing a sequential two-stage ε-constraint method coupled with a high-resolution (0.1-hour) weighted resource standard deviation metric, the framework strictly confines the optimization search within absolute engineering tolerance limits, yielding schedules that are both resource-level and practically viable for highly capital-intensive projects.
4. *Resilient rolling-horizon dynamic scheduling mechanism*: Bridging the gap between theoretical optimal and execution reality, a dynamic scheduling mechanism equipped with a precise multidimensional disturbance propagation model is developed. By simulating multi-scenario stochastic events, e.g., sudden geological variations, equipment breakdowns, and employing heuristic downstream task revocation, the framework enables continuous real-time schedule recovery and active makespan prediction, ensuring robust and stable project delivery under chaotic construction conditions.

2 Problem description and assumptions

2.1 Problem description

A dual-tunnel engineering project consists of S_d longitudinal segments. The excavation and initial support process flow for the entire cross-section is executed across distinct construction zones, the division of which is determined by the specific excavation method. For instance, under the three-bench seven-step excavation method, the cross-section is sequentially divided into seven construction zones. The set of construction zones is illustrated in Fig. 1 and denoted by G_ω. Tunnel construction activities comprise three distinct process flows: the excavation and initial support process flow, the inverted arch construction process flow, and the secondary lining process flow, denoted as W_{Exc}, W_{Inv} and W_{Lin} respectively. Each process flow contains a set of fixed operations, denoted as A_W. Specifically, the fixed operations within the excavation and initial support process flow $A_{W_{Exc}}$ are classified into five tasks: surveying, blasting/mechanical excavation, mucking and ventilation, initial support, and temporary support.

The tunnel excavation proceeds in a cyclic manner according to the construction zone sequence. The advancement of all construction zones by one foot length constitutes the completion of a single excavation cycle *r*. Within each construction zone, operations are

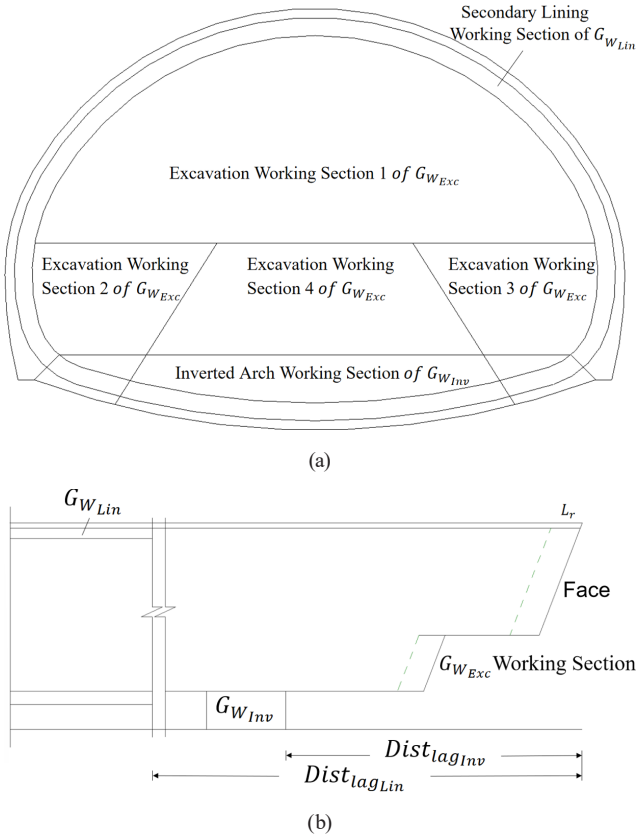

Fig. 1 Schematic diagrams of tunnel: (a) cross-section and (b) longitudinal section

performed cyclically following the sequence of fixed operations defined in the corresponding process flow set, as illustrated in Fig. 2. Compared to single-tunnel scheduling, dual-tunnel scheduling must additionally satisfy constraints regarding the minimum safety distance between the tunnel faces of the two tubes and the staggered utilization of shared resources.

2.2 Assumptions

The proposed scheduling model is developed under the following practical assumptions, which define the operational boundaries and resource sharing rules of the dual-tunnel construction:

1. The dual-tunnel are of the separated type, and their construction activities do not interfere with each other under the conditions of maintaining a specific mileage spacing of working faces and implementing peak-shifting use of shared resources.
2. For each activity within the same activity flow, the cyclic footage, duration, and resource demand per linear meter are set as fixed values and remain unchanged within a single cycle.
3. Different activity flows in a single tunnel can be constructed in parallel, while activities within the same activity flow are not constructed in parallel.
4. The left and right tubes of the tunnel maintain parallel construction and only share part of the key resources.
5. Tunnel construction is carried out as 24-hour continuous construction, adopting a three-shift system.

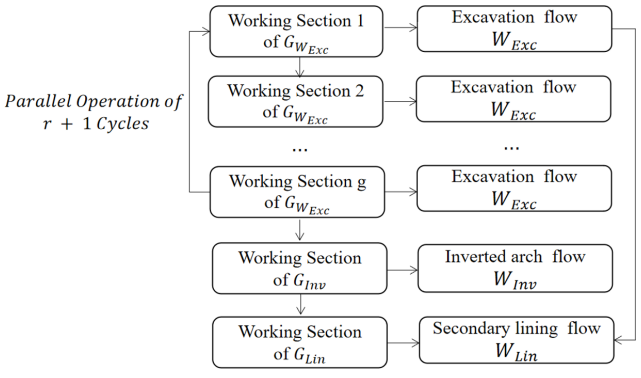

Fig. 2 Tunnel construction cycle flowchart

3 Mathematical model of scheduling optimization based on the ε-constraint method

3.1 Optimization objective 1: Minimizing total project duration

As expressed in Eq. (1), the first objective function is designed to minimize the total project duration:

$$\min C_{\max} \tag{1}$$

where $C_{\max}$ denotes the predicted maximum completion time of the project (i.e., the total project duration). This objective aims to minimize the total time required to complete all tasks.

To fundamentally prevent the algorithm from artificially delaying consecutive tasks to achieve mathematical resource smoothness—a phenomenon defined in this study as the idle penalty trap—a Dynamic Continuity Penalty Function ($\text{Penalty}_{\text{idle}}$) is introduced. In tunnel construction, operations within the same excavation cycle, e.g., drilling, mucking, support, must be executed seamlessly.

The penalized fitness makespan is mathematically defined as

$$\min F_1 = C_{\max} + \text{Penalty}_{\text{idle}}$$

$$\text{Penalty}_{\text{idle}} = \sum_{c \in C} \sum_{i,j \in A_c} \max\left(0, S_j - C_i\right) \cdot \lambda$$

where $C_{\max}$ is the absolute physical completion time; A_c represents the set of adjacent continuous operations within the same excavation cycle c; S_j and C_i are the start and

completion times of the successor and predecessor tasks, respectively. The λ is a dynamic penalty coefficient ($\lambda = 5.0$). This mechanism fiercely penalizes any non-physical gaps introduced between strictly continuous cyclic operations.

3.2 Constraints: Minimizing total project duration

3.2.1 General constraints

The total project duration must be greater than or equal to the completion time of any individual activity. Equation (2) formulates the fundamental duration constraint for each activity:

$$C_{\max} \geq C_i, \ \forall i \in I \tag{2}$$

where C_i denotes the planned completion time of activity i, and I represents the set of all activities. Each activity $i \in I$ is uniquely identified by a six-dimensional tuple (d, s, w, g, r, a), whose components represent the specific spatial and operational attributes. The parameters are sequentially defined as follows:

1. $d \in D$: The tunnel indicator, where $D = \{L, R\}$ represents the set of left and right tunnels.
2. $s \in S$: The specific longitudinal segment of the tunnel.
3. $w \in W$: The process flow, where $W = \{W_{Exc}, W_{Inv}, W_{Lin}\}$ represents the set of process flows (i.e., excavation and initial support, inverted arch, and secondary lining, respectively).
4. $g \in G_w$: The construction zone for a specific process flow w. The set G_w: is determined by the excavation method. For instance, in the two-bench four-step excavation method, the excavation zones are $G_{W_{Exc}} = \{1,2,3,4\}$, whereas the inverted arch and secondary lining each have only one zone, yielding $G_{W_{Inv}} = \{1\}$ and $G_{W_{Lin}} = \{1\}$.
5. $r \in R$: The index of the r^{th} construction cycle.
6. $a \in A_w$: The standard operation, where A_w defines the set of standard operations corresponding to process flow w.

For activities that have not yet started, their completion time equals their start time plus their duration according to Eq. (3):

$$C_i = S_i + p_i, \ \forall i \in I \text{ and } U_i = 1 \tag{3}$$

where S_i denotes the planned start time of activity $i \in I$; p_i is the estimated duration of activity $i \in I$; U_i is a binary parameter: it takes a value of 1 if activity i has not yet started at time T_{start}, and zero otherwise.

3.2.2 Initial state constraints for rolling optimization

During the dynamic scheduling process, the temporal boundary constraints must be categorized into three execution states to reflect the real-time construction status:

1. *For completed activities*:

$$S_i = S_i^{\text{actual}}, \ C_i = C_i^{\text{actual}}, \ \forall i \in I \text{ and } i \text{ is completed} \tag{4}$$

Where S_i^{actual} is the actual start time of activity i, obtained from recorded historical data; C_i^{actual} is the actual completion time of activity i.

2. *For ongoing activities*:

$$S_i = S_i^{\text{actual}}, \ C_i \geq S_i^{\text{actual}} + P_i^{\text{remain}}, \ \forall i \in I \text{ and } i \text{ is on going} \tag{5}$$

$$P_i^{\text{remain}} = P_i^{\text{updated}} - \left(T_{\text{start}} - S_i^{\text{actual}}\right) \tag{6}$$

Where P_i^{remain} denotes the remaining duration of activity i, which is input into the rolling optimization mechanism as an input parameter; P_i^{updated} is the updated estimated duration of activity i. During dynamic scheduling, events occurring in the previous cycle are reviewed: if construction changes occur, P_i^{updated} is updated; if no changes occur, $P_i^{\text{updated}} = p_i$; T_{start} is the start time of the current rolling optimization cycle; $T_{\text{start}} - S_i^{\text{actual}}$ represents the elapsed time from the actual start of activity i to the start of the current rolling optimization cycle.

3. *For all unstarted activities*:

The start time of any activity must be after the completion of all its preceding activities, aligning the model's calculation starting point with the project's actual status.

$$S_i \geq T_{\text{start}}, \ U_i = 1, \ \forall i \in I \tag{7}$$

$$S_j \geq C_i, \ \forall i \in P_i, \ \forall j \in I \tag{8}$$

Where P_i denotes the set of all preceding activities of activity $i \in I$.

3.2.3 Internal logical constraints of activity flows

The feasibility of the construction schedule relies on adhering to specific spatiotemporal restrictions. Section 3.2.3 details the internal logical constraints of the operations, dividing them into intra-cycle technological sequences and inter-section safety distance requirements:

1. *Intra-cycle constraints for activities*:

These constraints ensure that activities within the same cycle follow the technological sequence (e.g., surveying precedes excavation) and that the next cycle on the

same working face can only begin after the previous cycle is completed.

$$S_{(d,s,w,g,r,a)} \geq C_{(d,s,w,g,r,a-1)}, \quad \forall (d,s,w,g,r,a) \in I,\ \forall w \in W,\ a > 1 \tag{9}$$

Where $S_{(d,s,w,g,r,a)}$ and $C_{(d,s,w,g,r,a-1)}$ respectively represent the start time of activity a and the completion time of activity $a-1$, both within the same activity flow, same working section, and same cycle.

2. *Internal logical constraints of the excavation flow*:
   - Constraints for the initial phase of the excavation flow before entering cycles:
     To guarantee operational safety and prevent spatial interference, strict spatiotemporal constraints must be enforced between adjacent excavation working sections. The internal logical relationships of the excavation flow are modeled across two distinct stages as follows:
   - Constraints for the initial phase of the excavation flow before entering cycles:
     Logical constraints between different excavation working sections are established based on safety distances. These constraints ensure that a subsequent working section can only begin after the preceding working section has reached the safety distance. For each working section $g(g > 1)$ and its preceding working section g', Eq. (10) defines the internal activity constraints of the excavation flow:

$$S(d, W_{Exc}, g, 1, 1) \geq C(d, W_{Exc}, g', r^*, a_{\text{last}}) \tag{10}$$

where $A_{W_{Exc}}$ is the set of standard construction activities within a single excavation cycle, and $A_{W_{Exc}} = \{1,2,3,4,5\}$. Here, 1 represents surveying, 2 represents blasting/mechanical excavation, 3 represents muck removal and ventilation, 4 represents initial support, and 5 represents temporary support; r^* denotes the minimum cycle number that satisfies the condition $\sum_{k=1}^{r^*} L_k \geq Dist_{\text{ramp},g'g}$. The first cycle of working section g can only start after its preceding working section g' has completed an advance exceeding the safety advance distance $Dist_{\text{ramp},g'g}$; a_{last} is the last activity in the excavation activity set $A_{W_{Exc}}$.
   - Constraints for the steady-state phase of the excavation flow after entering cycles
     Constraints for the stable cycle phase take effect after all working sections are initiated. The safety distance between the subsequent working section g and its preceding working section g' maintains the spacing from the initial phase, and each activity in the excavation flow has the same footage. At this point, the cycle is updated to $r = 0$. For each working section $g(g > 1)$, its preceding working section g', and all cycles r and r':

$$S_{(d,W_{Exc},g,r,1)} \geq C_{(d,W_{Exc},g',r-1,a_{\text{last}})} + t_c \tag{11}$$

where $S_{(d,W_{Exc},g,r,1)}$ denotes the start time of the first activity in cycle r for working section g; $C_{(d,W_{Exc},g',r-1,a_{\text{last}})}$ is the completion time of a_{last} in the previous excavation cycle $r-1$ for the preceding working section g'; t_c represents the concrete curing time.

3.2.4 Logical constraints between activity flows

Following the activity logic of excavation leads, invert follows closely, secondary lining lags behind, dependency relationships between activity flows are established based on safety distances. For example, invert construction can only start after the excavation working face ahead of it has exceeded the safety distance, enabling staggered synchronous operation of different cross-sections. The types of safety distances are as follows:

1. *Safety distance between working face and invert flow*:

$$Pos_{d,W_{Exc},1,r_{\text{last}},1} - Pos_{d,W_{Inv},1,s_{\text{last}},1} \leq Dist_{lag_{Inv}},\ \forall d \in D \tag{12}$$

Where $Pos_{d,W_{Exc},1,r_{\text{last}},1}$ denotes the working face position of the first working section in the latest cycle r_{last} of the excavation flow (i.e., the working face); $Pos_{d,W_{Inv},1,s_{\text{last}},1}$ is the working face position of the working section in the latest cycle s_{last} of the invert flow; $Dist_{lag,Inv}$ represents the maximum safety distance between the working face and the invert working face.

2. *Safety distance between working face and secondary lining flow*:

$$Pos_{d,W_{Exc},1,r_{\text{last}},1} - Pos_{d,W_{Lin},1,t_{\text{last}},1} \leq Dist_{lag_{Lin}},\ \forall d \in D \tag{13}$$

Where $Pos_{d,W_{Lin},1,t_{\text{last}},1}$ denotes the working face position of the working section in the latest cycle t_{last} of the secondary lining flow; $Dist_{lag,Lin}$ is the maximum safety distance between the working face and the secondary lining working face.

3.2.5 Resource constraints

To prevent resource conflicts and over-allocation during the dual-tunnel construction, the schedule must strictly adhere to resource capacity limits. The resource constraints are formulated through a three-step process: defining the real-time execution status of each activity, calculating the cumulative periodic resource demand, and imposing an upper bound based on available capacity. The details of this three-step process are as follows:

1. *Definition of activity execution status*:

$$S_i \le t + M \cdot (1 - y_{it}) \forall i \in I,\ \forall t \in T \tag{14}$$

$$C_i \ge (t+1) - M \cdot (1 - y_{it}) \forall i \in I,\ \forall t \in T \tag{15}$$

$$\sum_{t \in T} y_{it} = p_i \ \forall i \in I \tag{16}$$

Where y_{it} is a binary variable that equals 1 if activity i is in progress at hour t, and 0 otherwise. If activity i has not started or has been completed by hour t, $y_{it} = 0$; M is a sufficiently large positive number, used to linearize the constraints.

2. *Calculation of periodic resource usage*:

$$u_{kt} = \sum_{\forall i \in I} r_{ik} \cdot y_{it},\ \forall k \in K,\ \forall t \in T \tag{17}$$

Where u_{kt} denotes the total usage of resource k at hour t; r_{ik} is the hourly demand of resource k for activity i; K is the set of all renewable resources (equipment, construction teams); T is the set of discretized time periods, where ($T = \{1, 2, \ldots, T_{\max}\}$)(unit: hour).

3. *Total resource constraint*:

$$u_{kt} \le Q_k,\ Q_k \ge 1,\ \forall k \in K,\ \forall t \in T \tag{18}$$

Where Q_k is the available quantity of resource $k \in K$.

3.2.6 Spatial coordination constraints for dual-tunnel construction

At any time, the longitudinal distance between the foremost working faces of the two tunnels shall not be less than a certain distance $\Delta D_{\min}$.

$$\left| Pos_{(L,s,\omega,g,r)} - Pos_{R,s,W_{Exc},g,r')} \right| \ge \Delta D_{\min},\quad \omega = \{1 | \omega \in W_{Exc}\},\ g = \{1 | g \in G_{W_{Exc}}\} \tag{19}$$

3.2.7 Definition of mileage calculation

To accurately track the spatial progression of the tunnel construction, the specific mileage position of an activity at the r^{th} cycle is determined by accumulating the lengths of all preceding excavation footages, as formulated in Eq. (20):

$$Pos_{(d,s,w,g,r,a)} = \sum_{k=1}^{r} L_k,\ r \in Z \tag{20}$$

where L_k denotes the footage length of the k^{th} excavation cycle (unit: meter).

3.3 Optimization objective and constraints for minimizing the weighted resource standard deviation

3.3.1 Optimization objective 2: Minimizing the weighted resource standard deviation

Traditional resource optimization often targets the absolute peak usage ($U_k^{\max}$). However, minimizing only the peak frequently leads to gradient distortion in multi-objective evolution, failing to penalize extreme day-to-day fluctuations below the peak. Therefore, this study adopts the Weighted Resource Standard Deviation to continuously evaluate the smoothness of resource allocation:

$$\min Z_2 = \sum_{k \in K} w_k \cdot \sigma_k \tag{21}$$

$$\sigma_k = \sqrt{\frac{1}{T_{\max}} \sum_{t=1}^{T_{\max}} (u_{kt} - \mu_k)^2} \tag{22}$$

where w_k denotes the weight of resource k, signifying its relative importance and scale constraint. The σ_k is the standard deviation of the utilization of resource k over the entire scheduling period, and μ_k is the average hourly consumption of resource k. By minimizing this objective, the algorithm mathematically flattens the resource usage curves, preventing sharp operational peaks and valleys.

3.3.2 Constraints: Minimizing the weighted resource standard deviation

Constraints for minimizing the weighted resource standard deviation include all constraints specified in Model 1. As expressed in Eq. (23), the constraint function is designed to limit the maximum resource usage.

$$U_k^{\max} \ge \sum_{t}^{\text{DAY}} u_{kt} \tag{23}$$

As expressed in Eq. (24), the ε-constraint function is designed to ensure that the total project duration does not exceed its optimal value by more than the relaxation factor ε:

$$C_{\max} \le (1 + \varepsilon) \cdot C_{\max}^{*} \tag{24}$$

where $C_{\max}^{*}$ denotes the benchmark optimal duration obtained from Model 1; ε is the duration tolerance coefficient,

a predefined dimensionless small value. It represents the maximum percentage of the model's duration that can be sacrificed in exchange for better resource leveling.

The adoption of this sequential ε-constraint strategy, rather than simultaneous bi-objective optimization, is driven by the physical reality of underground construction. In theoretical mathematics, simultaneous optimization algorithms treat both objectives with equal weight. To achieve a perfectly flat resource curve, such algorithms frequently delay non-critical (and sometimes critical) excavation tasks, creating artificial idle times. While the resource variance appears mathematically excellent, the absolute project duration extends far beyond acceptable engineering limits (the idle penalty trap). By optimizing time first to find the absolute minimum duration ($C^*_{\max}$), and then enforcing the ε-constraint tolerance, this model forces the algorithm to level resources strictly within an operationally viable timeframe, ensuring engineering practicality.

4 Algorithm design

To address the complexity of tunnel construction scheduling, this paper proposes a combined static and dynamic scheduling method, termed HGA-RHO (Hybrid Genetic Algorithm - Rolling Horizon Optimization). In the initial phase of the project, the HGA generates a static, globally optimal initial schedule (the baseline schedule). During project execution, a rolling-horizon optimization mechanism is used to dynamically reschedule periodically, thereby adapting to uncertainties encountered during construction.

4.1 Static global optimization via hybrid genetic algorithm (HGA)

While modern swarm intelligence metaheuristics (such as Particle Swarm Optimization or Whale Optimization Algorithm) have gained immense popularity in recent literature, our selection of a Genetic Algorithm (GA) framework is strictly dictated by the discrete topological nature of dual-tunnel construction. Continuous swarm algorithms rely on position-to-sequence mapping mechanisms (like Largest Order Value) for scheduling. When these algorithms update their continuous velocities or positions, they indiscriminately shatter the rigid spatial and physical locks of dual-tunnel construction, e.g., strict stagger distances between left and right tubes, leading to a catastrophic collapse in topological feasibility.

In contrast, the GA framework is natively discrete, allowing us to deeply embed domain-specific topological repair mechanisms directly into its genetic operators. Built upon the NSGA-II framework, our proposed Hybrid Genetic Algorithm (HGA) utilizes a customized precedence-preserving crossover and a workflow-aware smart mutation. It applies a local search strategy to elite individuals to enhance convergence speed while strictly maintaining the topological validity of the generated schedules. The ultimate goal is to obtain a Pareto-optimal solution set that minimizes both the total project duration and the Weighted Resource Standard Deviation.

4.1.1 Encoding and heuristic initialization

The algorithm employs a task priority-based permutation encoding scheme. A chromosome is represented as a sequence of task indices, where the position of a gene indicates the task's priority within the schedule. The initial population is generated using a novel Cycle-Aware Topological Initialization strategy. Conventional topological sorting generates purely random feasible sequences, which frequently fractures the tightly coupled operations within a single tunnel excavation cycle. To counter this, our initialization heuristically detects the cycle ID attribute of tasks. Once an excavation cycle is initiated, the generator strongly binds its subsequent intra-cycle tasks, e.g., mucking, temporary support, to form contiguous priority gene blocks in the chromosome. This domain-specific initialization not only guarantees to improve topological validity but inherently immunizes the initial population against severe gap-induced idle penalties from generation zero.

4.1.2 High-resolution decoding and generalized lag mapping

The decoding process employs a refined Serial Schedule Generation Scheme (SSGS) to transform the chromosome priority sequence into a feasible schedule. To overcome the discrete overlap bugs inherently caused by integer-hour modeling in conventional RCPSP, this study develops a High-Resolution Time Scale mechanism, configured at a 0.1-hour minute precision.

First, all operations are initialized as unscheduled. The earliest start time for each task is calculated utilizing a Generalized Lag Mapping framework, which converts conventional Precedence Relations into a dictionary matrix accommodating exact spatial lag times ($Lag_{i,j}$). Specifically, the earliest start time ES_j for task j is strictly bounded by $\max(C_i + Lag_{i,j})$ for all predecessors i. Subsequently, an adaptive step-size mechanism performs high-precision resource availability checks across the 0.1 hour resolution arrays. Upon completing scheduling,

the algorithm decodes the absolute physical makespan and calculates the fitness values based on the penalized duration and resource standard deviation.

4.1.3 Crossover and mutation operators

The algorithm adopts the Order Crossover (OX) operator. A gene segment from parent chromosome P_1 is randomly selected and directly inherited by offspring chromosome C_1. The remaining positions in C_1 are filled sequentially with genes from the other parent (e.g., P_2) that are not included in the inherited segment. The dual offspring is generated in the same manner by swapping the parents' roles. This crossover method (Fig. 3) maximally preserves the superior subsequence structures of the parents without disrupting the relative order of tasks, significantly reducing the probability of generating infeasible solutions.

To preserve structural feasibility while maximizing search explosiveness, a Workflow-Similarity-Based Smart Mutation operator is proposed. Standard random point mutations blindly swap task indices, frequently violating the spatial sequences of tunneling and generating infeasible chromosomes. Instead, our operator employs a dual-mechanism: with a 50% probability, it triggers a global shuffle for aggressive exploration; with the remaining 50%, it executes an intelligent homologous substitution. It identifies the workflow attribute, e.g., left-tunnel excavation vs right-tunnel excavation, of the target gene and exclusively swaps its priority with another task belonging to the identical workflow type. This mechanically sound perturbation allows the algorithm to safely heuristically alter resource contention priorities between parallel tubes without rupturing the intra-tube physical sequences.

4.1.4 Elite local search strategy

The algorithm gives strict priority to minimizing the project duration; reducing the Weighted Resource Standard Deviation is considered only when the durations of candidate solutions are identical.

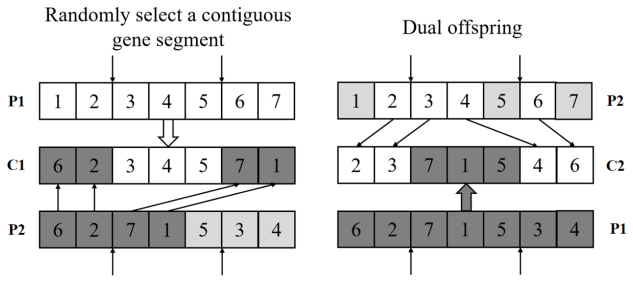

Fig. 3 Chromosome crossover method

In the initial stages, the population fully explores the solution space through crossover and mutation operators. Upon reaching a specified generation count, elite individuals identified during the global search are selected to undergo a Hill-Climbing local search, subject to a predefined local search probability. The number of search iterations is adaptive, effectively controlling the search depth.

The neighborhood operations alternately employ swap moves and insert moves. Specifically, these operations involve randomly swapping the positions of two tasks or removing a task and inserting it into a different position within the sequence. This strategy ensures sufficient perturbation of the task sequence, facilitating the escape from local optima and accelerating convergence towards high-quality solution regions. The acceptance criterion adopts Lexicographical Order to evaluate the fitness of neighborhood solutions. If a generated neighboring solution outperforms the original elite individual, the elite is replaced.

4.2 Dynamic scheduling optimization mechanism based on rolling horizon

While static optimization yields an ideal, globally optimal schedule, it is inadequate for addressing unforeseen external disturbances encountered during actual construction, such as abrupt changes in surrounding rock conditions or variations in construction efficiency due to equipment failures.

Therefore, this paper proposes a dynamic scheduling optimization method based on the Rolling Horizon approach. By integrating Discrete Event Simulation (DES) with a heuristic resource-constrained scheduling algorithm, the proposed method can simulate two distinct dynamic scenarios: standard-duration disturbances and sudden resource breakdowns. This framework facilitates continuous decision-making in construction, alongside dynamic schedule optimization, enabling the assessment of the impact of disturbance events on project progress.

4.2.1 Simulation clock advancement and disturbance injection in rolling horizon

The dynamic scheduling optimization framework employs a simulated global clock that advances cyclically with a fixed time step. At the commencement of each simulation cycle, the status of project tasks is evaluated and categorized into one of four mutually exclusive states: Completed, In-process, Scheduled, or Unscheduled. When one or more disturbance events are triggered, the system selects the specific tasks to be disturbed by sorting them

based on spatiotemporal priority. Subsequently, disturbance parameters are injected to simulate real-world conditions. The exact steps are as follows:

1. *Disturbance triggering*: The occurrence of a disturbance event is controlled by verifying whether its predetermined trigger time, *T*, is less than or equal to the current simulation clock time.
2. *Candidate selection*: All tasks currently in the In-process, Scheduled, or Unscheduled states at the disturbance time point are aggregated to form a set of candidate tasks.
3. *Priority sorting*: Candidate tasks undergo multidimensional spatiotemporal priority sorting. Based on this priority, the target task located within the disturbance event window is selected. Factors influencing priority include task status, start time, and longitudinal segment (mileage).
4. *Parameter injection*: The corresponding disturbance coefficients are injected into the selected target task. This mechanism ensures that disturbances are invariably applied to the most immediate task, thereby accurately simulating the physical process of disturbances propagating along the tunnel face.

4.2.2 Disturbance response model

Section 4.2.2 introduces the disturbance response model designed to simulate real-world uncertainties during the construction process. Specifically, the model addresses two primary categories of dynamic disruptions: variations in production efficiency due to geological changes, and temporary resource shortages caused by equipment failures. The detailed response mechanisms and propagation rules for these two scenarios are formulated as follows:

1. *Production efficiency disturbances and cascading propagation*: To address disturbance events that directly impact operation duration—such as abrupt changes in surrounding rock class, forced work stoppages, and rework—and to simulate the physical authenticity of these disturbances, specific disturbance events are defined using the following control parameters: window hours, disruption factor (*F*), disrupt time, and rework ratio. In particular, given that disturbances caused by changes in geological conditions exert varying degrees of impact depending on the task status and excavation zone, an additional penalty is applied explicitly on top of the baseline disruption factor *F* to reflect this heterogeneity. The specific operation to be disturbed is identified by sequentially sorting candidate tasks based on spatiotemporal priority. Priority is assigned to tasks that are currently in process, have earlier start times, are located at lower mileage (earlier longitudinal segments), and appear earlier in the process sequence. When a task's duration is extended, delaying its completion, the system recursively checks all scheduled successor tasks. If a conflict arises (i.e., the finish time of the disturbed predecessor *i* exceeds the planned start time of its successor *j*), the successor task is forcibly postponed. This recursive check continues for the subsequent successors, ensuring that the delay effect propagates thoroughly throughout the precedence network.
2. *Temporary resource shortage disturbance and task cancellation mechanism*: In response to a sudden reduction in resource supply due to equipment failures, the affected resource's available capacity is immediately reduced to the failure level, and a specific recovery time is designated.

For tasks currently in progress: If a task is currently consuming the affected resource, a work stoppage (waiting period) is immediately imposed until the resource becomes available or recovers. For scheduled but unstarted tasks: Regarding tasks that are planned but have not yet commenced during the failure window, if their projected resource demand exceeds the reduced capacity limit, their status is reset to unscheduled. Consequently, all their successor tasks are recursively revoked and returned to the unscheduled pool. This mechanism effectively simulates a partial schedule breakdown resulting from resource shortages, necessitating the rescheduling of subsequent tasks where appropriate.

4.2.3 Heuristic local scheduling strategy

The dynamic scheduling decision-making process focuses exclusively on tasks scheduled to commence within the current time window. Once the propagation of disturbance effects is complete, tasks that have reverted to an unscheduled status are re-inserted into the timeline.

To minimize computational overhead, the full HGA is not re-invoked during this phase. Instead, the method adopts a strategy that mimics the population initialization step in the HGA, using neighborhood heuristic rules to sort candidate tasks. Priority is assigned to tasks located on the critical path and those positioned earlier in the sequence.

For these high-priority tasks, the system performs a search using a small time step within the window

to identify the earliest feasible start time that satisfies resource constraints (accounting for resources currently allocated to other scheduled tasks). This mechanism effectively emulates the HGA's decoding process. Subsequently, the simulation clock rolls forward by one time step, transitioning the system into the next iteration cycle.

4.2.4 Real-time duration prediction and performance evaluation

To ensure dynamic visibility of the project status, the system predicts and records the final state of the entire project. Upon completion of scheduling in each simulation cycle, a rapid forward-pass calculation using the Critical Path Method (CPM)—with relaxed resource constraints—is performed for all remaining incomplete tasks based on the currently scheduled tasks.

This process predicts the project's final completion time and Weighted Resource Standard Deviation, which are then recorded in the historical log. These records provide a basis for subsequent analysis of schedule robustness, evaluation of duration deviations caused by disturbances, and implementation of timely corrective actions.

5 Case verification

5.1 Case data

This study validates the proposed method using a specific dual-tunnel highway project as a case study. The construction organization design covers the sections from ZK27+415 to ZK27+515 (Left Tube) and YK27+404 to YK27+504 (Right Tube). The Two-Bench Four-Step excavation method is adopted for construction. Consequently, the workflow comprises four excavation construction zones, five standard excavation operations, one inverted arch construction zone, and one secondary lining construction zone. The project involves a total of 3,412 operations: 3,360 excavation, 34 inverted arch, and 18 secondary lining. The project utilizes 12 distinct types of resources. Based on the project's specific construction scheme and the Chinese standard "JTG F90-2015 Safety Technical Specifications for Highway Engineering Construction" [35], the basic construction design parameters are presented in Table 1. Furthermore, statistical data derived from construction ledgers and design documents regarding the average construction rate per linear meter, resource demand, and resource capacity limits for each operation are detailed in Table 2.

5.2 Static and dynamic optimization schemes

The proposed Hybrid Genetic Algorithm (HGA) and the rolling optimization algorithm were executed with the following parameter configurations: a population size of 120, 140 generations, a crossover probability of 0.8, and a mutation probability of 0.2. Six sets of Pareto optimal solutions (Pareto Front) were obtained from the optimization process. Each scheme represents a feasible optimal solution derived under a specific trade-off preference (balancing time and resources). The corresponding relationship between Total Duration and Weighted Resource Standard Deviation is illustrated in Fig. 4.

Among the solutions obtained, Fig. 5 represents the optimal solution characterized by the shortest duration, achieving a Fitness Makespan of 223.3 day, Physical Makespan of 122.2 day and the Weighted Resource Standard Deviation of 37.88. Furthermore, project managers can select the most appropriate scheme based on the specific urgency or trade-off preferences regarding project duration versus resource

Table 1 Basic parameters of actual construction

			Duration (h/m)				
	Safety distance	Cycle footage	Surveying	Blasting/Mechanical excavation	Mucking and ventilation	Initial support	Concrete curing
Excavation zone 1		1.2 m	0.45	3.24	0.54	0.648	168
	3~5 m						
Excavation zone 2		1.2 m	0.45	1.62	0.27	0.324	0
	2.5~3 m						
Excavation zone 3		1.2 m	0.45	1.62	0.27	0.324	0
	2~3 m						
Excavation zone 4		1.2 m	0.4	1.68	0.27	0	0
Inverted arch zone	Distance to face ≤ 40 m	6 m			5		
Secondary lining zone	Distance to face ≤ 60 m	12 m			4		

Table 2 Resource requirements for labor, materials, and equipment

	Resource weight	Excavation zone 1	Excavation zone 2	Excavation zone 3	Excavation zone 4	Inverted arch zone	Secondary lining zone	Total resource limit Q_k
Surveying team	0.1	1	0	0	0	0	1	4
Workers	0.2	9	4	4	3	12	12	130
Steel	0.05	868.4	104.7	104.7	0	1212.7	946.5	50000
Concrete	0.2	7.5	0.78	0.78	0	27.38	14.42	50000
Excavator	0.01	1	1	1	1	1	0	5
Loader	0.05	1	1	1	1	1	0	4
Mucking truck	0.05	4	4	4	4	4	0	16
Wet shotcrete machine	0.05	1	1	1	0	0	0	3
Concrete mixer truck	0.05	2	1	1	0	4	4	8
Excavation trolley	0.05	1	0	0	0	0	0	4
Waterproofing trolley	0.05	0	0	0	0	0	2	2
Lining gantry	0.05	0	0	0	0	0	2	2

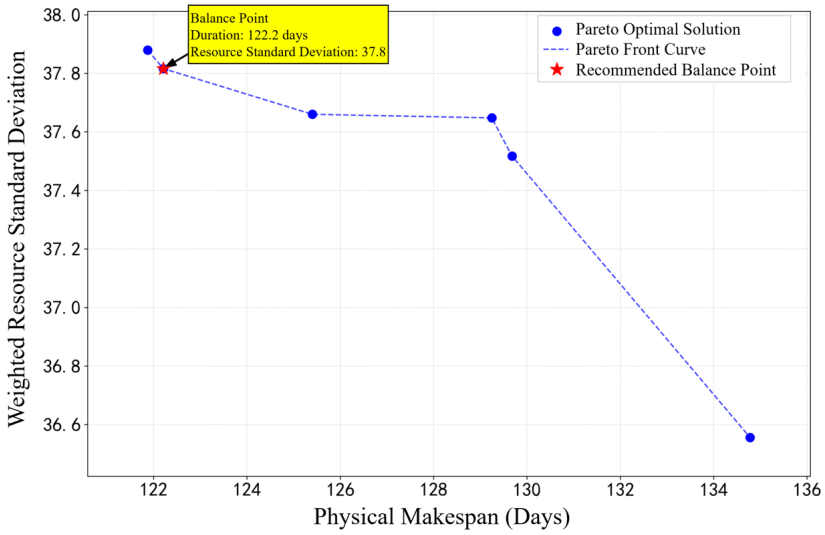

Fig. 4 Pareto curve of static optimization

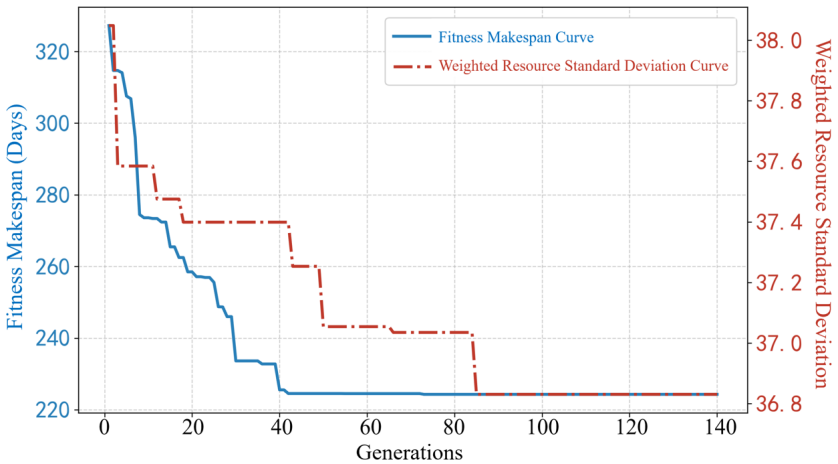

Fig. 5 The multi-objective convergence curve of the HGA algorithm

leveling. Linear scheduling method static optimization for dual-tunnel construction scheduling is illustrated in Fig. 6. As observed in Fig. 6, the construction progress curves for the left and right tubes remain generally parallel, exhibiting a coordinated construction rhythm and tight sequencing between operations. Furthermore, the constraints

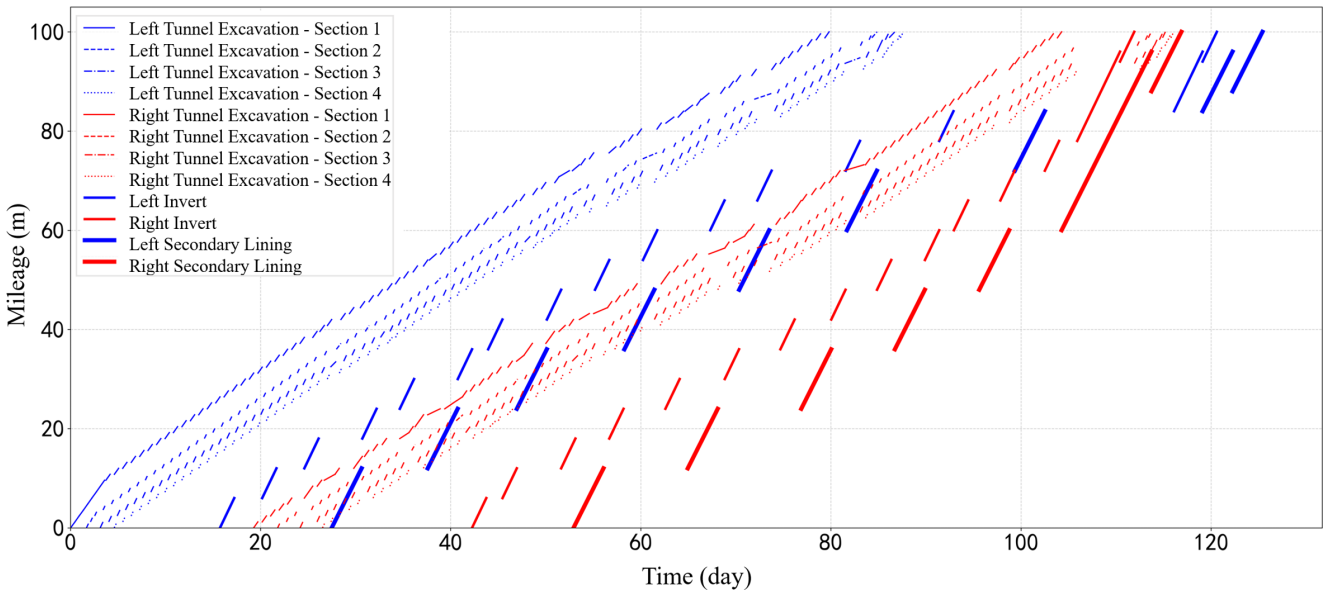

Fig. 6 Linear scheduling method static optimization for dual-tunnel construction scheduling

regarding the minimum safety distance between adjacent operations are strictly satisfied, thereby demonstrating the effectiveness of the spatiotemporal constraints incorporated into the proposed model.

5.3 Analysis of optimization strategies

To rigorously justify the adoption of the sequential ε-constraint method over traditional simultaneous multi-objective optimization, a comparative analysis of their solution spaces was conducted. We evaluated a pure NSGA-II approach—which simultaneously minimizes project duration and resource standard deviation—against the solutions derived from the proposed ε-constraint HGA ($\varepsilon = 0.15$). As illustrated in Fig. 7, the simultaneous optimization approach generates a highly dispersed mathematical Pareto front. To achieve marginal reductions in resource fluctuations, pure NSGA-II frequently resorts to severely extending the total project duration, which is completely unviable in highly capital-intensive tunnel projects.

In the purely physical perspective illustrated in Fig. 7 (a), despite a generous tolerance margin of approximately 18 days between the minimum duration and the ε-tolerance limit, the optimal solutions generated by the HGA do not disperse toward the right. Although this 15% physical relaxation mathematically permits schedule delays for the sake of resource leveling, the workflow interruptions induced by such delays incur exorbitant idle penalties. Consequently, these discontinuous pseudo-optimal schedules are rigorously eliminated during the comprehensive evaluation shown in Fig. 7 (b). Fig. 7 (b) reveals the engineering reality through a comprehensive evaluation perspective, which strictly incorporates idle penalties to penalize workflow interruptions. Certain optimal solutions derived from the ε-constraint method left of the minimum duration boundary. This phenomenon arises because the first stage minimizes the comprehensive makespan, which explicitly incorporates idle penalties. During the second-stage search, the algorithm further compresses the purely physical timeline through aggressive task overlapping. However, this compression inevitably induces more severe idle penalties. Since their total comprehensive durations still remain within the permissible $(1 + \varepsilon)$ boundary, these solutions are preserved as valid alternatives. Therefore, the ε-constraint method compels the HGA to level resources exclusively by fine-tuning the priorities of parallel tasks while strictly preserving construction continuity, ultimately achieving the lowest possible resource variance. This empirically proves that the ε-constraint method is fundamentally necessary to bridge the gap between abstract mathematical optimality and the strict spatiotemporal realities of dual-tunnel construction.

5.4 Comprehensive Algorithm Benchmarking and Mechanism Analysis

To rigorously evaluate the superiority and necessity of the proposed Customized HGA, a comprehensive benchmark was conducted against four representative optimization algorithms: Standard NSGA-II, Multi-Objective Whale Optimization Algorithm (MOWOA), Simulated Annealing (SA), and Particle Swarm Optimization (PSO).

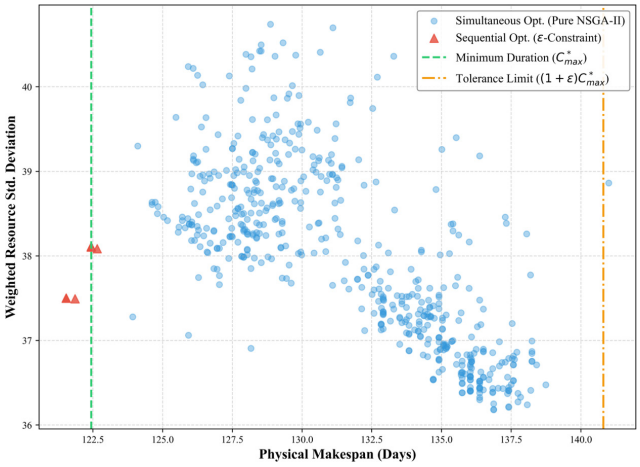

(a)

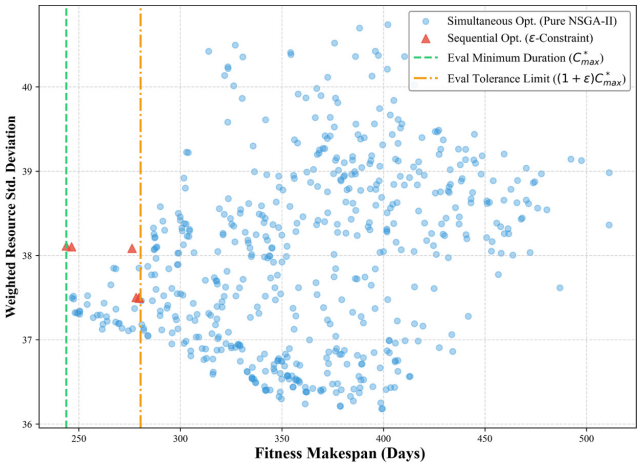

(b)

Fig. 7 Comparison of solution spaces between simultaneous and sequential optimization strategies: (a) Physical makespan evaluation perspective, (b) Fitness makespan evaluation perspective

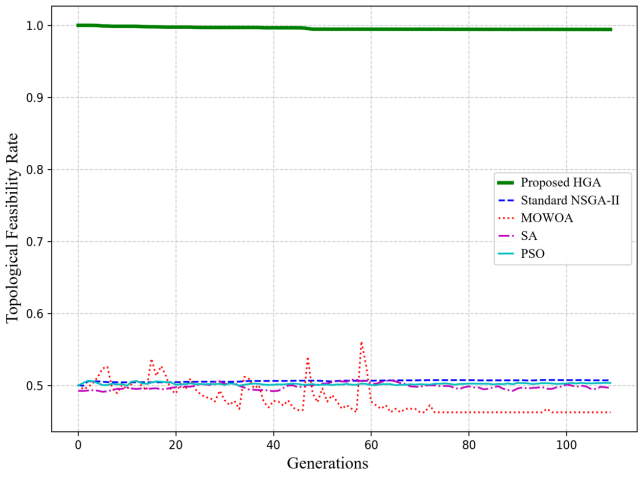

(a)

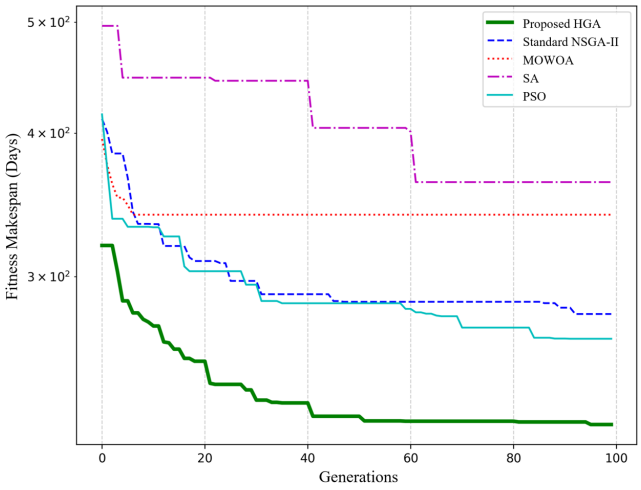

(b)

Fig. 8 Performance evaluation of optimization algorithms for (a) Feasibility rate of task sequences, (b) Fitness makespan performance and (c) Physical makespan performance

To ensure absolute computational fairness, all algorithms utilized identical population sizes, generation limits, and decoding scheme.

Benchmarking results as Fig. 8 reveal a critical incompatibility between continuous swarm intelligence algorithms and strict precedence-constrained scheduling:

1. *Topological feasibility collapse*: As shown in Fig. 8 (a), MOWOA and PSO exhibit a near-zero feasibility rate throughout the iterations. Their continuous position updating mechanisms, when mapped back to discrete sequences, fundamentally shatter the complex topological network of dual-tunnel construction. They exhaust vast computational resources evaluating invalid sequence combinations.
2. *The idle penalty bottleneck*: Fig. 8 (b) illustrates the convergence of the fitness makespan (incorporating penalties for resource waiting). Standard discrete algorithms (NSGA-II and SA) bypass the continuous mapping trap but struggle to eliminate high idle penalties. Their generic random mutation operators frequently fragment the tightly coupled sequential tasks within a single excavation cycle, causing dependent tasks to be interrupted by other out-of-order activities. In stark contrast, the proposed HGA consistently dominates the benchmark, maintaining a high feasibility rate and ultimately converging to the absolute optimal physical makespan as Fig. 8 (c). This overwhelming superiority is strictly attributed to its domain-specific genetic operators. The Cycle-aware Topological Initialization inherently immunizes the population against gap-induced idle penalties, while the Workflow-Similarity-based Smart Mutation restricts genetic swaps to tasks with equivalent engineering logic. This equips the HGA with aggressive exploratory power while acting as an impenetrable shield against cycle-breaking penalties.

5.5 Comprehensive performance comparison of static and dynamic optimization algorithms

The static optimization results serve as the theoretical benchmark, whereas the rolling-horizon dynamic optimization simulates the periodic dynamic updating of the schedule and duration forecasts as construction progresses. For the rolling horizon dynamic scheduling strategy, the time step was set to 1 day. Under ideal conditions without disturbances, the predicted total project duration is 125.6 days. To evaluate the solution quality, efficiency, and stability of the proposed algorithms, a comparative analysis was conducted among the Genetic Algorithm (GA), Hybrid Genetic Algorithm (HGA), and the Rolling Horizon algorithm using the aforementioned case study. The statistical results of 25 independent runs for each algorithm are shown in Table 3.

The results demonstrate that the HGA exhibits a significant improvement in optimization stability regarding project duration compared to the standard GA. The rolling-horizon dynamic scheduling optimization is significantly superior to the HGA in terms of stability and computational cost, though it is slightly inferior in global optimality. Nevertheless, compared to the actual project completion duration of 139 days, the two methods achieved duration reductions of 13.3% and 11.5%, respectively.

5.5.1 Sensitivity analysis of disturbance timing

To investigate the adaptability of scheduling schemes under different conditions and the sensitivity of disturbance timing, four distinct disturbance scenarios were defined and injected at three different stages of the project lifecycle: Early, Middle, and Late (measured in days). These scenarios were compared against the Ideal Scenario (free of external disturbances) to analyze the dynamic response characteristics of the rolling horizon optimization in handling sudden disturbances. The experiment examines the system's immediate reaction to disturbance shocks, the evolutionary trajectory of long-term predictions, and the stability of resource utilization.

Table 3 Comparison of results between static and dynamic optimization

	Duration (days)	Weighted Resource Standard Deviation	Computing time (s)	Standard deviation
GA	148.72	36.08	689.62	12.61
HGA	123.10	38.88	671.09	1.87
RH (Ideal)	125.60	47.16	28.40	0

The parameters for the construction disturbance scenarios are as follows: Scenario A (Geological Change): a reduction in construction rate due to sudden changes in geological conditions. The disturbance impact factor F is set to 1.5 (the duration of affected tasks is extended to 1.5 times the original planned duration). Scenario B (Forced Stoppage): Construction stagnation caused by a forced work stoppage. The stoppage duration is 48 hours, with a disturbance event window of 1 hour. Scenario C (Quality Rework): Rework caused by quality non-conformance. The rework ratio is 0.5 (the duration of affected tasks is extended by 50% of the original planned duration)—scenario D (Equipment Failure): A decrease in efficiency caused by equipment failure. The failure is simulated on an excavator, resulting in a 50% reduction in total production capacity. Note: The disturbance event windows for Scenarios A, C, and D are all set to 72 hours.

Fig. 9 illustrates the spatiotemporal-resource coupling characteristics of dual-tube tunnel construction based on rolling horizon optimization under ideal scenarios. The chart maps the Linear Scheduling Method (LSM) diagram and the predicted resource smoothness onto a shared time axis. This multidimensional visual integration intuitively reveals the dynamic squeezing effect of spatial topological constraints on global resource scheduling flexibility during the construction process.

The evolutionary trajectory of resource smoothness exhibits a high degree of causal coupling with the spatial unlocking process of the working faces. This evolution can be primarily delineated into three stages:

1. *Initial high-degree-of-freedom peak-shaving period (Days 0–20)*: During the early construction phase, only the excavation of the left tunnel face (L-Tunnel Excavation) proceeds as a single workflow. Devoid of spatial entanglements from subsequent activities, the heuristic algorithm possesses significant scheduling elasticity (slack time) within the rolling horizon. Through staggered scheduling, the algorithm successfully achieves peak-shaving and valley-filling within the working parts, driving the resource standard deviation down sharply from an initial 48 to a nadir of approximately 31, thereby reaching a theoretically optimal state of resource equilibrium.
2. *Spatial constraint triggering and resource deterioration period (Days 20–80)*: As the excavation mileage accumulates, a series of rigid physical constraints are triggered. Around Day 20 and Day 40, having

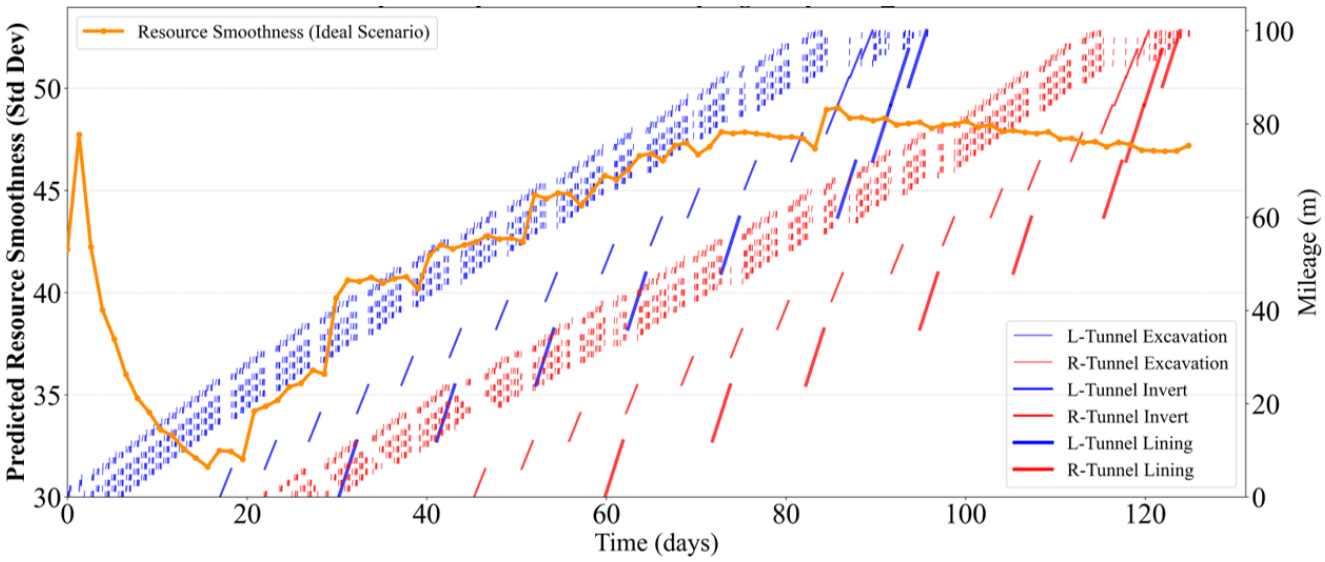

Fig. 9 Dynamic evolution analysis of spatiotemporal-resource coupling in the dual-tube tunnel under the ideal scenario

satisfied the single-tube maximum lag constraints (preventing operational detachment) and the dual-tube minimum stagger constraints (preventing blasting interference), the invert and lining activities of both tunnels are mandatorily unlocked in succession. As depicted in Fig. 9, the take-off of each new activity line in the background precisely corresponds to a step-like leap in the upper bright orange curve. This phenomenon indicates that, to satisfy the stringent topological shackles, high-energy-consuming tasks are forced into overlapping time windows. Consequently, the algorithm's peak-shaving solution space undergoes step-wise compression, leading to an irreversible physical deterioration of resource smoothness.

3. *Fully-loaded steady state and tail-end convergence period (Day 80 to completion)*: After Day 80, the red and blue lines representing the six core workflows of both tunnels fully intertwine, indicating that the tunnel construction has entered a fully-loaded steady state. At this point, the complexity of the spatial network topology reaches its peak, and the resource fluctuation forms an oscillating plateau in the high-value range of 45–50. In the tail-end period of the project (after Day 100), as the excavation operations successively achieve breakthrough, the most stringent face-pulling constraints are lifted. The withdrawal of high-energy-consuming equipment releases scheduling elasticity, prompting a gentle downward convergence of the resource standard deviation curve.

Figs. 10–12 illustrate the trends in the predicted total duration, the duration deviation between the ideal and disturbed scenarios, and the Weighted Resource Standard Deviation as the rolling-horizon simulation clock advances under different disturbance types and timings. Figs. 10–12 intuitively reflect the optimization strategy of dynamic scheduling: compensating for the impact of disturbances by re-coordinating the duration and resource usage of various operations.

When a disturbance is applied during the early construction phase (as illustrated in Fig. 7, where it occurs at $T = 30$), its impact propagates widely across subsequent operations. Although the immediate rescheduling of subsequent tasks is prompt and subtle, the magnitude of the impact progressively amplifies as time advances.

This phenomenon can be attributed to the fact that early disturbances primarily affect tunnel excavation tasks. Since the duration of a single excavation cycle is relatively short, short-term coordination is manageable. However, as the project progresses and an increasing number of operations commence simultaneous execution, the accumulation of initially minor impacts results in more significant fluctuations.

Nevertheless, since resource utilization has not yet reached its peak capacity at this stage, the heuristic scheduling strategy can effectively leverage resource buffers and the free float (slack time) of non-critical tasks to absorb the shock. This demonstrates the proposed dynamic scheduling approach's ability to recover from disturbances during the early stages.

When disturbances are introduced during the intermediate construction phase (at $T = 60$, as illustrated in Fig. 8), the

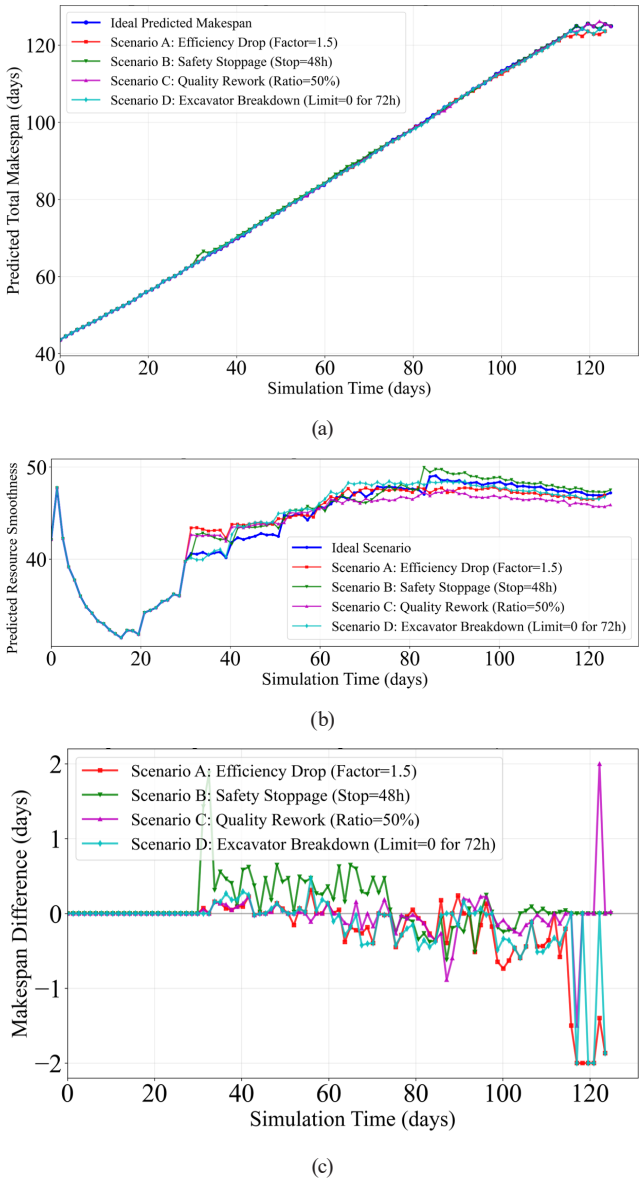

Fig. 10 (a) Prediction of duration and (b) Weighted resource leveling, and (c) Duration variation analysis under disturbance on Day 30

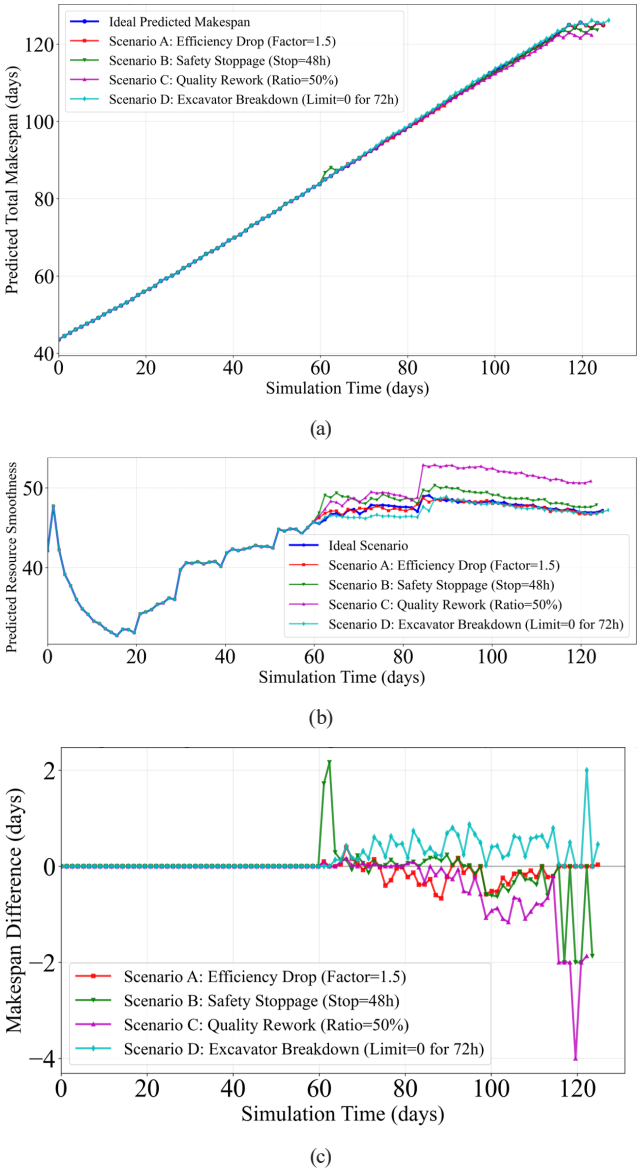

Fig. 11 (a) Prediction of duration and (b) Weighted resource leveling, and (c) Duration variation analysis under disturbance on Day 60

variations in both project duration and weighted resource standard deviations within the current time window are significantly amplified. This phenomenon is attributed to the concurrent advancement of multiple operations, including excavation, inverted arch construction, and secondary lining. Consequently, a substantial variety and quantity of resources are currently occupied, causing the system to operate in a state nearing its resource capacity limits. Under such tight constraints, even minor disturbances trigger extensive adjustments to subsequent tasks, exerting a relatively severe impact on the overall construction process.

When disturbances are introduced during the late construction phase (at T = 100, as shown in Fig. 8), the fluctuation in project duration decreases compared to the intermediate phase but remains significant. This is attributed to the fact that the construction of the left tube has been fully completed by this stage, leaving only the tasks for the right tube to be executed. Consequently, the number of tasks available for scheduling is reduced, and resource demand becomes relatively concentrated. Under these conditions, the impact of disturbances on extending the project duration remains pronounced.

Table 4 reveals that under complex spatial constraints, the impact of dynamic disruptions on the total makespan exhibits highly nonlinear temporal characteristics. The magnitude of the impact depends not on the absolute severity of the disruption, but rather relies heavily on the spatiotemporal network state at the time of triggering:

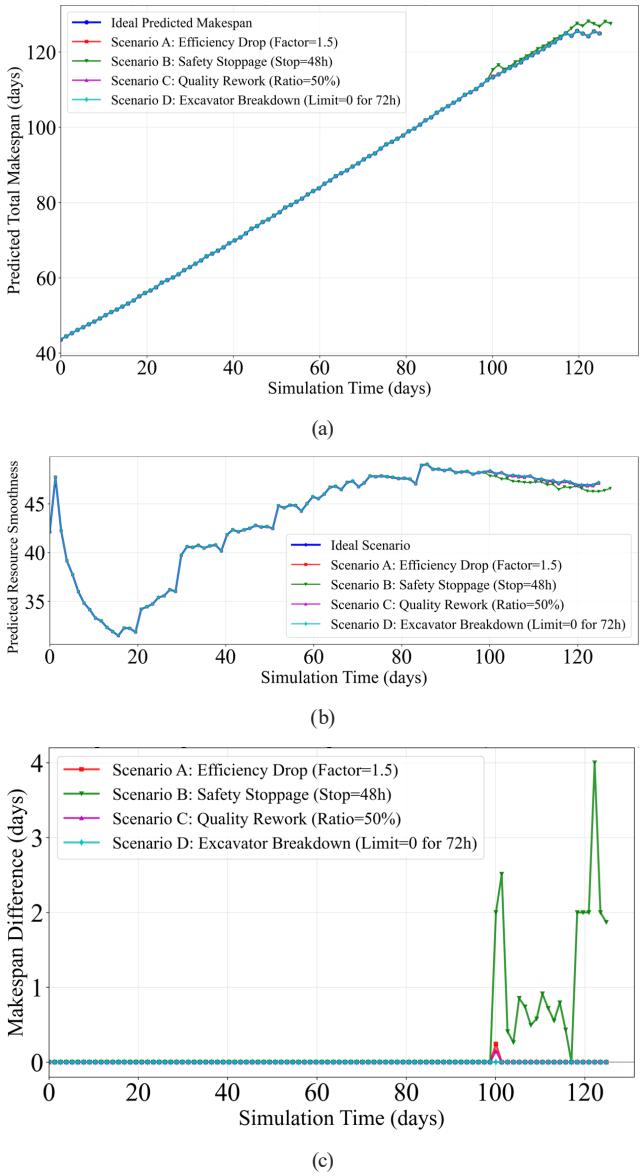

Fig. 12 (a) Prediction of duration and (b) Weighted resource leveling, and (c) Duration variation analysis under disturbance on Day 100

1. *High-degree-of-freedom period (T = 30)*: Perturbation optimization effect. During the early construction phase, the system possesses abundant slack time. Disruptions (e.g., Scenarios A and D) do not cause delays but act as perturbation operators, forcing the heuristic algorithm to escape local optima, dynamically reorder the cut-in sequence of the subsequent invert and lining activities. Capitalizing on the high initial degrees of freedom, the algorithm not only absorbs the disruption entirely but also serendipitously discovers a more compact resource-leveling sequence, achieving perturbation optimization.
2. *Fully-loaded steady state (T = 60)*: Day 60 represents the fully-loaded steady state, where all six workflows of the dual tubes comprehensively intertwine. Synchronization barrier effect. At this stage, the dual-tube spatial stagger constraints strictly compress the scheduling solution space. While efficiency drops cause significant delays, specific forced stoppages (e.g., Scenarios B and C) physically act as synchronization barriers. These barriers forcefully align the spatial steps of subsequent working faces, effectively reducing future fragmented idle time within the system, thereby triggering makespan reductions again.
3. *Tail-end convergence period (T = 100)*: At Day 100, the tunnel face excavation is essentially broken through, high-energy-consuming equipment is withdrawn, and the project enters the wrap-up phase dominated by invert and lining operations. Since excavation is complete, disruptions targeting excavation efficiency (A), rework (C), or excavator availability (D) fail to impact the critical path and are effectively neutralized. However, Scenario B is an indiscriminate safety stoppage. In the final stage of the project, almost all remaining tasks reside on the critical path. With a forced 48-hour standstill, the system is left with zero subsequent slack time to absorb the delay. Consequently, this 48-hour stoppage is converted at a nearly 1:1 ratio into an irreversible makespan delay.

Table 4 Predicted duration values under four scenarios at three distinct disturbance time points

	Scenario A	Scenario B	Scenario C	Scenario D
Disrupted $T = 30$	124.7	125.6	125.6	124.7
Difference from ideal case	−1.8	0	0	−1.8
Disrupted $T = 60$	125.6	124.6	124.6	126.1
Difference from ideal case	3.2	−1.9	−1.9	0.5
Disrupted $T = 100$	125.6	127.5	125.6	125.6
Difference from ideal case	0	1.9	0	0

6 Conclusions

Addressing the characteristics of multi-cycle operations and multi-spatial constraints in dual-tunnel construction, this paper develops a high-fidelity multi-objective scheduling optimization model to minimize both the total project duration and Weighted Resource Standard Deviations,

the traditional fixed duration–resource leveling problem is re-engineered through a micro-spatiotemporal lens. A comprehensive tunnel scheduling optimization framework is established by integrating HGA-based static optimization with Rolling Horizon-based dynamic scheduling. The specific conclusions are summarized as follows:

1. The proposed Hybrid Genetic Algorithm (HGA) successfully eliminates the pervasive issue of topological deadlocks in narrow spaces. Furthermore, a fine-grained time-slice mapping mechanism is embedded to eradicate microscopic resource fragmentation. Algorithmically, the HGA significantly enhances the global exploration boundary through an unbiased topological sequence initialization, while ensuring intra-cycle operational continuity via a dynamic penalty function. By integrating elite local search operators, the algorithm effectively overcomes genetic hardening. The static optimization results for the 100 m dual-tunnel case reduced the construction duration by 13.3% compared to the actual duration, generating a uniformly distributed Pareto front that offers a diverse trade-off between speed and resource leveling.
2. To address uncertainties in actual tunnel construction, a heuristic scheduling strategy within the Rolling Horizon framework is adopted. This approach delivers rapid scheduling decisions while ensuring logical correctness and resource feasibility. Under ideal conditions, the dynamic optimization predicted an 11.5% reduction in duration compared to the actual 142 days. While this strategy entails a trade-off in global optimality, it demonstrates significant advantages in terms of computational efficiency and the capability to handle uncertainties.
3. Experiments were conducted by simulating the dynamic characteristics of various disturbance types and injecting disturbances of varying magnitudes into the rolling horizon dynamic scheduling. Experimental results indicate that the duration prediction curves for all scenarios maintained a stable linear growth trend without catastrophic divergence. This verifies the stability and overall robustness of the dynamic optimization mechanism in regulating the construction rhythm under disturbance conditions.

References

[1] Ministry of Transport of the People's Republic of China "2024 年交通运输行业发展统计公报" (2024 Statistical Communique on the Development of the Transportation Industry), Ministry of Transport of the People's Republic of China, Beijing, China, 000019713O04/2025-00029, 2025. [online] Available at: https://xxgk.mot.gov.cn/2020/jigou/zhghs/202506/t20250610_4170228.html (in Chinese)

[2] Pan, Z., Zhou, G., Huang, C. "基于IGSA的线性工程施工进度计划优化模型研究" (Research on Optimization Model of Linear Engineering Construction Schedule Planning Based on IGSA), Chinese Journal of Management Science, 33(07), pp. 210–221, 2025. (in Chinese) https://doi.org/10.16381/j.cnki.issn1003-207x.2022.1627

[3] Tang, Y. J. "交通运输线性工程施工进度计划编制及优化方法研究" (Research on Compilation and Optimization Methods of Transportation Linear Engineering Construction Schedule), PhD Thesis, Beijing Jiao Tong University, 2015. (in Chinese)

[4] Duffy, G., Woldesenbet, A., Jeong, D. H. S., Oberlender, G. D. "Advanced linear scheduling program with varying production rates for pipeline construction projects", Automation in Construction, 27, pp. 99–110, 2012. https://doi.org/10.1016/j.autcon.2012.05.014

[5] Zhou, G., Zhang, H. "基于多工作面的铁路特长隧道施工进度计划优化" (Optimization of Construction Schedule of the Railway Extra-long Tunnel Based on Multiple Working Faces), Operations Research and Management Science, 32(09), pp. 21–27, 2023. (in Chinese)

[6] Su, R., Aviles, J. S. "Construction Scheduling Optimization of Prefabricated Buildings Under Resource Constraints Based on an Improved Whale Optimization Algorithm", International Journal of Computational Intelligence Systems, 18(1), 166, 2025. https://doi.org/10.1007/s44196-025-00898-1

[7] Peng, J., Wang, M. "Optimizing Scheduling for Emergency Public Response Projects Amid Resource Variability", KSCE Journal of Civil Engineering, 29(11), 100268, 2025. https://doi.org/10.1016/j.kscej.2025.100268

[8] Pham, V. H. S., Truong, T. T. H. "Mountain Gazelle Optimization algorithm for efficient rebar cutting: balancing material cost and waste in construction projects", KSCE Journal of Civil Engineering, 30(1), 100322, 2026. https://doi.org/10.1016/j.kscej.2025.100322

[9] Dede, T., Sin, T. S., Yılmaz, M., Uçan, H. A., Rao, R. V. "Integrated risk management in construction project: utilizing NDSII-BMR and NDSII-BWR for time-cost-safety trade-offs", Engineering Computations, 43(1), pp. 292–325, 2026. https://doi.org/10.1108/EC-04-2025-0339

[10] Yılmaz, M., Dede, T. "Optimizing Multiobjective Time–Cost–Quality Problems in Construction Projects: Efficacy of Strength Pareto-Based Rao Algorithms", Journal of Construction Engineering and Management, 151(5), 04025036, 2025. https://doi.org/10.1061/JCEMD4.COENG-15551

[11] Guo, K., Zhang, L. "Multi-objective optimization in tunnel line alignment under uncertainty", Automation in Construction, 122, 103504, 2021. https://doi.org/10.1016/j.autcon.2020.103504

[12] Ren, J., Zhang, Y. "Multi-objective optimization in the renewal of historic and cultural neighborhoods: application to Shenyang's Bagua street using an improved NSGA-II algorithm", KSCE Journal of Civil Engineering, 29(10), 100214, 2025. https://doi.org/10.1016/j.kscej.2025.100214

[13] Albayrak, G. "Optimizing of Discrete Time-cost Trade-off Problem in Construction Projects Using Advanced Jaya Algorithm", Periodica Polytechnica Civil Engineering, 67(3), pp. 806–818, 2023. https://doi.org/10.3311/PPci.22156

[14] Yu, D., Lv, Q., Srivastava, G., Chen, C.-H., Lin, J. C.-W. "Multi-objective evolutionary model of the construction industry based on network planning", IEEE Transactions on Industrial Informatics, 19(2), pp. 2173–2182, 2022. https://doi.org/10.1109/TII.2022.3190566

[15] Kaveh, A., Shirzadi Javid, A. A., Vazirinia, Y. "Multi-objective Variants of Water Strider Algorithm for Construction Engineering Optimization Problems", Periodica Polytechnica Civil Engineering, 69(3), pp. 925–943, 2025. https://doi.org/10.3311/PPci.40442

[16] Kaveh, A., Mahdavi, V. R. "Multi-objective colliding bodies optimization algorithm for design of trusses", Journal of Computational Design and Engineering, 6(1), pp. 49–59, 2019. https://doi.org/10.1016/j.jcde.2018.04.001

[17] Kaveh, A., Fahimi-Farzam, M., Kalateh-Ahani, M. "Performance-based multi-objective optimal design of steel frame structures: Nonlinear dynamic procedure", Scientia Iranica, Transactions A: Civil Engineering, 22(2), pp. 373–387, 2015.

[18] Kaveh, A., Laknejadi, K., Alinejad, B. "Performance-based multi-objective optimization of large steel structures", Acta Mechanica, 223(2), pp. 355–369, 2012. https://doi.org/10.1007/s00707-011-0564-1

[19] Song, M., Lin, J., Liu, X., Jia, H., Luo, S. "Octopus optimization algorithm: a novel single- and multi-objective optimization algorithm for optimization problems", Cluster Computing, 28(8), 484, 2025. https://doi.org/10.1007/s10586-025-05141-2

[20] Kaveh, A., Rajabi, F. "Fuzzy-multi-mode Resource-constrained Discrete Time-cost-resource Optimization in Project Scheduling Using ENSCBO", Periodica Polytechnica Civil Engineering, 66(1), pp. 50–62, 2022. https://doi.org/10.3311/PPci.19145

[21] Hu, W., Zhang, Y., Liu, L., Zhang, P., Qin, J., Nie, B. "Study on Multi-Objective optimization of construction project based on improved genetic algorithm and particle swarm optimization", Processes, 12(8), 1737, 2024. https://doi.org/10.3390/pr12081737

[22] Zou, H., Zhou, G. "多梁场铁路桥梁架梁工程调度优化模型与混合遗传算法" (Optimization model and hybrid genetic algorithm for beam erection project of railway bridge in multi beam yard), Operation Research Transactions, 2025. (in Chinese)

[23] Pham, V. H. S., Dau, T. D., Nguyen, V. H. "A Modified Dragonfly Algorithm for Solving the Temporary Facility Location Planning Problem in Construction Sites", KSCE Journal of Civil Engineering, 29(12), 100275, 2025. https://doi.org/10.1016/j.kscej.2025.100275

[24] Kaveh, A., Shirzadi Javid, A. A., Vazirinia, Y. "Physics-inspired Metaheuristics for Construction Site Layout Planning Problem", Periodica Polytechnica Civil Engineering, 68(1), pp. 68–87, 2024. https://doi.org/10.3311/PPci.22902

[25] Asadianfam, S., Emami, H. "An adaptive seasons optimization algorithm for global optimization", The Journal of Supercomputing, 81(9), 1048, 2025. https://doi.org/10.1007/s11227-025-07511-4

[26] Wang, H., Zhang, H., Lin, W., Pan, A., Zhu, C., Zhang, L. "Welding sequence optimization based on BP and chaotic whale optimization", Welding in the World, 2025. https://doi.org/10.1007/s40194-025-02232-x

[27] Wang, Y., Xu, C., Xie, H., Yang, J., Sheng, Z. "A novel path planning algorithm for virtual disassembly of components within aircraft fuel tanks", Engineering Optimization, 2025. https://doi.org/10.1080/0305215X.2025.2562360

[28] Zheng, K., Liu, H., Li, B. "Improved Snake Optimization Algorithm for Global Optimization and Engineering Applications", Scientific Reports, 15(1), 18171, 2025. https://doi.org/10.1038/s41598-025-01299-2

[29] Cheng, Y., Zhang, P., Liu, X. "Collaborative autonomous optimization of interconnected multi-energy systems with two-stage transactive control framework", Energies, 13(1), 171, 2020. https://doi.org/10.3390/en13010171

[30] Zan, Y., Liu, G., Wang, C., Zhang, W., Liu, X., Zhong, Z., Zhang, J. "并行异速机批量混合流水车间动态调度方法研究" (Dynamic scheduling method of lot-streaming hybrid flow shop scheduling problem with uniform parallel machines), Journal of Mechanical & Electrical Engineering, 43(1), pp. 102–116, 2026. (in Chinese) https://doi.org/10.3969/j.issn.1001-4551.2026.01.011

[31] Wei, R., Zhang, Z., Zhang, K., Gou, X., Zhu, X. "Development and application of dynamic configuration and intelligent scheduling system for drilling and blasting tunnel construction equipment", Tunnelling and Underground Space Technology, 168, 107164, 2026. https://doi.org/10.1016/j.tust.2025.107164

[32] Zhang, J., Zhan, Y., Cao, Y. "Research on Aviation Route Optimization Model Based on Dynamic Programming", In: 2024 4th International Signal Processing, Communications and Engineering Management Conference (ISPCEM), Montreal, QC, Canada, 2024, pp. 230–236. ISBN 979-8-3315-2868-3 https://doi.org/10.1109/ISPCEM64498.2024.00047

[33] Khallaf, Z., Alshibani, A., Alsawafy, O., Mohammed, A., Bubshait, A. "Dynamic Fleet Configuration Model for Optimizing Earthmoving Operations Using Mixed Integer Linear Programming", Journal of Construction Engineering and Management, 150(11), 04024152, 2024. https://doi.org/10.1061/JCEMD4.COENG-14817

[34] Wei, J., Liu, Y., Lu, X., Zhao, R., Wang, G. "Dynamic Optimization of Tunnel Construction Scheduling in a Reverse Construction Scenario", Systems, 13(3), 168, 2025. https://doi.org/10.3390/systems13030168

[35] JT "JTG F90-2015 Safety Technical Specifications for Highway Engineering Construction", Ministry of Transport of the People's Republic of China, Beijing, China, 2015.